Traveling Wave Ion Mobility Mass Spectrometry and Ab Initio Calculations of Phosphoric Acid Clusters

Hélène Lavanant, Vincent Tognetti, Carlos Afonso

Travelling Wave Ion Mobility Mass Spectrometry and *Ab Initio* Calculations of Phosphoric Acid Clusters

Hélène Lavanant,* Vincent Tognetti, Carlos Afonso

Normandie Univ, COBRA, UMR 6014 et FR 3038; Université de Rouen; INSA de Rouen; CNRS, IRCOF, 1 rue Tesnière, 76821 Mont-Saint-Aignan Cedex, France.

* Corresponding author
Université de Rouen,
IRCOF, 1 Rue Tesnière,
76821 Mont-Saint-Aignan Cedex, France
Tel: +33 2 35 52 29 32
helene.lavanant@univ-rouen.fr.

DOI : 10.1007/s13361-013-0818-3

Abstract

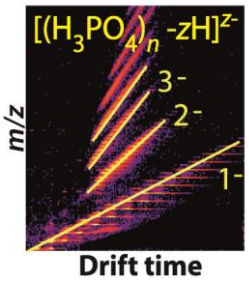

Positive and negative ion electrospray mass spectra obtained from 50 mM phosphoric acid solutions presented a large number of phosphoric acid clusters: $[(H_3PO_4)_n + zH]^{z+}$ or $[(H_3PO_4)_n - zH]^{z-}$, with *n* up to 200 and *z* up to 4 for positively charged clusters, and *n* up to 270 and *z* up to 7 for negatively charged cluster ions. Ion mobility experiments allowed very explicit separation of the different charge states. Because of the increased pressures involved in ion mobility experiments, dissociation to smaller clusters was observed both in the trap and transfer areas. Voltages along the ion path could be optimized so as to minimize this effect, which can directly be associated with the cleavage of hydrogen bonds.

Having excluded the ion mobility times that resulted from dissociated ions, each cluster ion appeared at a single drift time. These drift times showed a linear progression with the number of phosphoric atoms for cluster ions of the same charge state.

Cross section calculations were carried out with MOBCAL on DFT optimized geometries with different hydrogen locations and with three types of atomic charges. DFT geometry optimizations yielded roughly spherical structures. Our results for nitrogen gas interaction cross sections showed that values were dependent on the atomic charges definition used in the MOBCAL calculation. This pinpointed the necessity to define a clear theoretical framework before any comparative interpretations be attempted with uncharacterized compounds.

Received: 13 November 2013/Revised: 20 December 2013/Accepted: 21 December 2013/Published online: 6 February 201

Introduction

Unlike with conventional uniform field ion mobility, the use of calibrants is required with travelling wave ion mobility (TWIMS) to derive collision cross sections (CCS) values from the measured drift-times [1-7]. The CCS determination is essential to infer structural information from drift times in ion mobility–mass spectrometry, and there is now considerable interest to use this additional information as a means to characterize complex mixtures in many diverse "-omic" areas of study [8-10]. For positive ions, many calibrants exist, from which CCS was previously determined experimentally, with helium as the drift gas. Most of these calibrants are protonated biological molecules [11]. The conformations of these species are not always well defined, however, and they are highly dependent on experimental conditions [4,12,13]. The use of native-like proteins have been shown to be interesting to avoid such problems but they can be used only for large molecular systems [4]. Furthermore, there are, at present, few references in the literature concerning IMS in the negative ion mode and with nitrogen as drift gas [2]. An additional concern is that despite the progress and the increase in reference data, there is still, at this day, no consensus as to calibration methods and calibrants for travelling wave ion mobility [2-4].

Inorganic and organic cluster ions have been extensively investigated by mass spectrometry [14-20] and some of them are used for calibration of mass analyzers as they can yield ions covering a large mass range [21]. Such clusters are indeed readily produced using direct infusion of salt solution with an electrospray ion source.

Here, we performed travelling wave ion mobility mass spectrometry of phosphoric acid cluster ions. Cluster ions have been investigated by ion mobility mass spectrometry, but were mostly salt clusters [22-26]. In solution, phosphoric acid tends to aggregates as it presents both proton donor and acceptor sites [27,28]. Phosphoric acid clusters are hydrogen bonded cluster ions and should therefore be more closely related to non-covalent biomolecule complexes. Phosphoric acid was the topic of several recent theoretical and experimental studies [28-30]. The rationale for these investigations is related to the properties of phosphoric acid clusters and their use for development of electrolyte for fuel cells [29,31].

We show here how the use of hydrogen bonded cluster ions may be valuable to optimize experimental parameters that promote the retention of hydrogen bonds in the gas phase. Using these optimized experimental parameters, we studied the arrival time distributions of negatively charged intact cluster ions with increasing cluster size. In the absence of reference cross section data for small molecules in the negative mode, density functional theory calculations were carried out in order to optimize the geometries of the first six cluster ions and estimate theoretical cross sections, as has been done before by others [32-34] on small molecules, in the positive ion mode. Correlations were then tested between our experimental data and the calculated cross sections

Experimental

Chemicals

The phosphoric acid used was an 85% weight solution in water (d=1.680) from Acros Organics (through Fisher Scientific France, Illkirch, France). 3-nitrobenzyl alcohol (*m*-NBA) and sulfolane were purchased from Sigma-Aldrich (Lyon, France). LC-MS grade acetonitrile and isopropanol were purchased from VWR (Fontenay-sous-bois, France). Deionized water (18 MΩ) was obtained from a Milli-Q apparatus (Millipore, Bedford, MA, USA). 50 mM solutions were prepared in water/acetonitrile 50/50 and water/acetonitrile 50/50 (0.35% volume of the phosphoric acid solution). Supercharging agent *m*-nitrobenzyl alcohol (*m*-NBA) was added up to 1% volume in some cases.

Ion mobility mass spectrometry

Ion mobility and mass spectra were obtained using a SYNAPT G2 HDMS (Waters Corp., Manchester, UK) fitted with an electrospray ionization source. ESI mass spectra were acquired over the *m/z* 50-4000

range. In the positive and negative ion modes, absolute values for the capillary emitter were 2.7 kV and sampling cone 60 V. The source temperature was set at 90°C. Nitrogen gas at a temperature of 250°C and a flow rate of 500 L/h was used to assist desolvation in the ESI source. The solution was infused at a flow rate of 5 µL/min using the spectrometer sample pump. Gas flow rates were set at 20 mL/min in the source stacked ring ion guide, 180 mL/min in the helium cell and 70 mL/min in the ion mobility cell. Trap and transfer collision energies were set to 5 V and 0 V respectively. Travelling wave velocities were most often set around 300-350 m/s and the wave height at 15 to 25 V, to minimize hydrogen bond disruption. Direct current voltages in the trap and IMS cells were also adjusted to minimize fragmentation. Data treatment was carried out with Mass Lynx (4.1) and Driftscope (2.2).

Computational details

Ab initio calculations were carried out within density functional theory (DFT) using the Gaussian09 software [35], the dispersion-corrected range-separated hybrid ωB97XD exchange-correlation functional (whose parameters were optimized notably for non-covalent interactions) [36] and 6-31++G(d,p) basis set. Geometry from a recent crystal structure [37] was used as starting point. It was obtained from the Inorganic Crystal Structure Database (ICSD, FIZ Karlsruhe, Germany)[38,39]. Starting from a multiple cell (2a,2b,2c), an inner phosphoric acid molecule and its five nearest neighbors were selected. From this neutral 6-mer, the adequate number of phosphoric acid molecules was deleted following a decreasing distance in order to generate the smaller clusters. From these neutral clusters, all possible 3*n* hydrogen positions (*n* is the number of phosphorus atoms in the cluster) were tested as possible deprotonation sites. The conformational space of the negatively charged clusters was therefore sampled with 3*n* geometries for each *n*-mer.

Cross section calculations were carried out with slightly modified versions of MOBCAL [40,41] in both helium (mass 4.0026 u and polarizability 0.205 10^{-30} m^3) and nitrogen gas (mass 28.01 u and polarizability 1.71 10^{-30} m^3) . Lennard-Jones (LJ) parameters were adapted from Campuzano *et al.* [42] except for phosphorus for which the Lennard-Jones parameters were set equal to the existing values for silicon. The number of trajectories were increased both for the enhanced hard sphere scattering and trajectory methods (imp=1500 and inum=2500000). As a result standard deviations on the trajectory method were less than 1%.

Results

Optimization of experimental parameters

The process of acquiring ion mobility mass spectrometry data involves an increase of pressure in the IMS SRIG (TWIM) which is usually set in the mbar range compared to the values used for regular time-of-flight analysis which are more often a little lower than 10^{-4} mbar in this area. As a result, the pressure readbacks increase in the two stacked ring ion guides (SRIG) named trap and transfer from around 10^{-4} mbar to more than 10^{-2} mbar. When the instrument is switched from the time-of-flight mass spectrometry mode to ion mobility mass spectrometry mode, ion transmission and dissociation dramatically change as illustrated on figure 1. The mass spectra shown in figure 1 were recorded to test how these increases of pressure and voltage settings in the two ion guides adjacent to the ion mobility device might affect the transmission of one ion chosen as an example, a negatively charged hexamer $[(H_3PO_4)_6–H]^-$ (*m/z* 586.85). This was carried out in the time-of-flight mode (*i.e.* without activating the ion mobility mode), after mass selection through the quadrupole; the gas in the trap or transfer cells was thus argon rather than a mixture of helium and nitrogen gas leaking from the neighboring TWIM cell, which was here maintained at low pressure. Figure 1a shows that with low pressures, collision energies set to 10V and 5V in the trap and transfer SRIG had no effect on cluster dissociation as the negatively charged hexamer

$[(H_3PO_4)_6–H]^-$ (*m/z* 586.85) remained the sole ion observed.

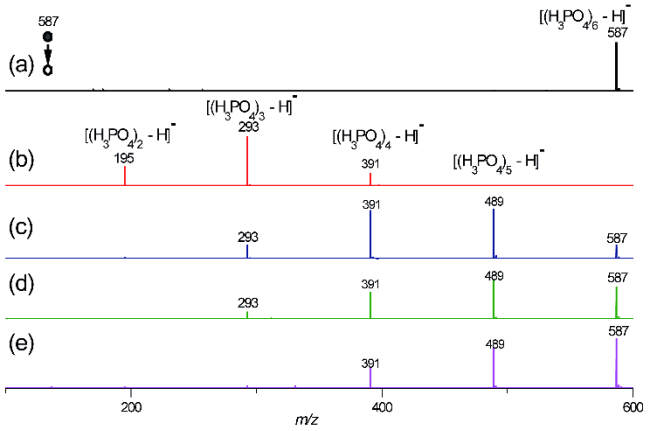

Fig. 1 ESI MS^2 of $[(H_3PO_4)_6 – H]^-$ (*m/z* 586.85) (a) Trap CE 5V, transfer CE 10V, trap and transfer pressure 10^{-4} mbar (TOF pressures); (b) trap CE 5V, transfer CE 10V, trap and transfer pressure 10^{-2} mbar (IMS pressures); (c) trap CE 5V, transfer CE 0V, trap and transfer pressure 10^{-2} mbar (IMS pressures); (d) trap CE 2V, transfer CE 0V, trap and transfer pressure 10^{-2} mbar (IMS pressures), trap bias 0 V; (e) trap CE 2V, transfer CE 0V, trap and transfer pressure 10^{-2} mbar (IMS pressures), trap bias 0 V, IMS bias 1.0 V

When pressures were set around the ion mobility mode readbacks in the trap and transfer SRIG, all hexamer anions were dissociated (figure 1b). Although the center of mass energy with argon collisions is expected to be higher than with helium or nitrogen gas, this showed activation should be anticipated in the ion mobility mode from the passage of the ions through these increased pressure areas. By setting the transfer collision energy at 0V, the dissociation occurring in the transfer SRIG could be reduced (figure 1c). An additional decrease in activation could be obtained by lowering the trap collision and DC bias voltage (figure 1d) and IMS bias voltage (figure 1e).

Control of the amount of dissociation was found to have very significant effect on the peak profiles in the ion mobility spectra. Figure 2 shows several ion mobility spectra obtained from experiments with different transfer or trap collision energies and DC bias voltages. Here, no mass selection was carried out in the quadrupole. When the ion mobility mode was switched on, without any change in instrumental parameters other than setting the wave velocity (WV) and wave height (WH) in the IMS SRIG, several resolved or unresolved peaks could be observed (figures 2a and 2b) in the arrival time distribution (ATD) of *m/z* 586.

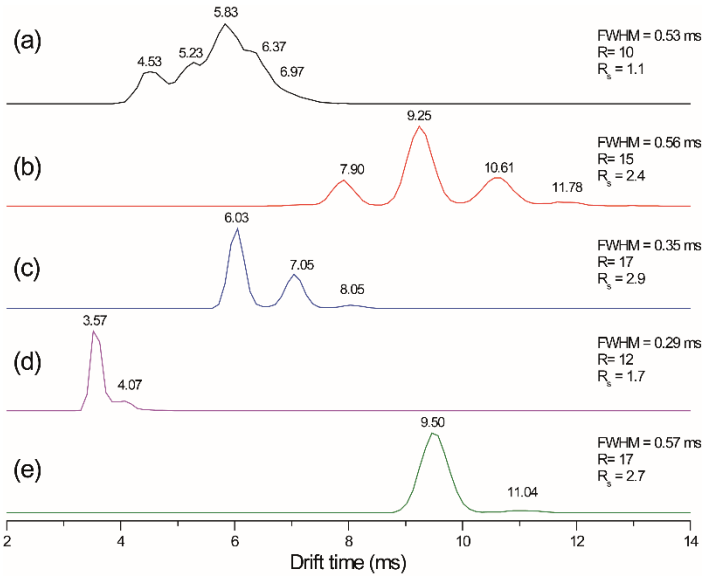

Fig. 2 Extracted ion drift time data of $[(H_3PO_4)_6 – H]^-$ (*m/z* 586.85) (a) IMS: WV 1000 m/s, WH 25V, transfer (default values): WV 191 m/s, WH 4.0 V, CE 10 V; (b) IMS: WV 800 m/s, WH 25V, transfer: WV 800 m/s, WH 4.0 V, CE 0 V; (c) IMS: WV 600 m/s, WH 25V, transfer: WV 600 m/s, WH 5.0 V, CE 0 V; (d) IMS: WV 350 m/s, WH 25V, transfer: WV 350 m/s, WH 5.0 V, CE 0 V; (e) IMS: WV 350 m/s, WH 15V, transfer: WV 350 m/s, WH 5.0 V, CE 0 V, lowered trap DC bias and IMS bias (40V and 0V respectively). FWHM refers to the full width at half maximum, R is the ratio of drift time to FWHM, and R_s is the ratio the drift time difference of two adjacent peaks to the FWHM

Comparison of ATDs for selected *m/z* of several cluster ions (7-mer, 8-mer, 9mer) showed overlapping of peaks for all drift time values except for the shortest drift times (data not shown). Most peaks in these extracted ion drift time profiles could

therefore be attributed to precursor ions of the negatively charged hexamer $[(H_3PO_4)_6–H]^-$. Indeed, rather than several conformations, a significant part of the signals detected in the ion mobility spectra corresponded to larger cluster ions for which dissociation occurred after the ion mobility device (in the transfer SRIG) and before the *m/z* analysis in the orthogonal time-of-flight analyzer.

When mass selection was carried out in the quadrupole, the arrival time distribution of *m/z* 586 did not show any signal from these precursor. In this case the extent of dissociation could be determined from the total ion mobility spectrum, as it was not apparent in the extracted ion mobility spectrum. This would need to be done for each precursor ion whereas without selecting in the quadrupole, all data can be retrieved from one experiment.. When no mass selection in the quadrupole was used, peak attribution in the ion mobility spectra was sometimes ambiguous when ion activation was significant after the TWIM device. Our objective was therefore to obtain one unique peak that could unambiguously be attributed to intact ions.

This was achieved by decreasing all values of wave velocity, wave height and collision energy in the trap, ion mobility and transfer ion guides (Figure 2c and 2d). Lower wave velocity yielded lower drift time as the ions rolled less over the wave [43], while the intensity increase of the lower drift time peak in the distribution showed that there was less dissociation. In Figure 2, the m/z 586.85 hexamers formed by the dissociation of larger clusters after the IM separation produced the higher drift time values, whereas, the intact hexamer should correspond to the peak with the lowest drift time. It is worth noting that the ion mobility spectra in Figure 2 are analogous to precursor ion scan spectra of *m/z* 586.85. Low proportion of dissociation and good resolving power were achieved with 350 m/s WV and 15V WH, similar WV and low WH were applied to the trap and transfer SRIG, no collision energy was used in the transfer SRIG and trap and IMS bias voltages were set at low values (Figure 2e). In Figure 2e the signal at 9.50 ms corresponded to the intact hexamer at *m/z* 586.85.

This data was consistent with effective temperature estimations by Morsa *et al.* [44]. Classically, experimental parameters affect the energy of collisions with gas molecules. Here, the dissociation of phosphoric acid cluster ions, which are hydrogen-bonded clusters, pointed out to the possibility of disruption or retention hydrogen bonds in the gas phase with different instrumental settings. It seemed very likely that such cleavage of hydrogen bonds would also occur in peptides and proteins, thereby modifying their gas phase conformation. For peptides and proteins however, the absence of dissociation would not make the cleavage of hydrogen bonds apparent, unless measurements of collision cross sections with different experimental parameters were carried out. The use of phosphoric acid cluster ions, on the other hand clearly underlined the parameters that enabled retention of these non-covalent interactions.

Ion mobility

Figure 3 shows examples of color maps of *m/z* versus arrival time data, obtained in the positive and negative ion modes with the previously described optimized parameters. The green dots outline the signals of phosphoric acid cluster ions (monoisotopic ions). With supercharging agent *meta*-nitrobenzyl alcohol [45], multiply charged cluster ions $[(H_3PO_4)n+zH]^{z+}$ or $[(H_3PO_4)n–zH]^{z-}$ could be observed with *n* up to 200 and *z* up to 4 for positively charged clusters, and *n* up to 270 and *z* up to 7 for negatively charged cluster ions.

Cluster ions of a given charge state formed well separated diagonal lines in the color maps. For one *m/z* value, peaks at several drift times could be observed, particularly in the low mass range. As described before, the higher drift time peaks corresponded to larger clusters that dissociated in the transfer SRIG, and showed a typical “time-aligned” pattern [46,47]. The lower drift time peak was the most intense and could be attributed to the intact cluster. Figure 4 shows the correlation obtained between the lower drift time bin and the cluster number *n*. R^2 values were almost all above 0.99. This

high correlation showed the potential of phosphate cluster ions for the calibration of cross sections versus drift time associated with measurements in traveling wave ion mobility devices [2,4,5,48,49]. Unfortunately, no experimental collision cross sections of phosphoric acid cluster currently exist.

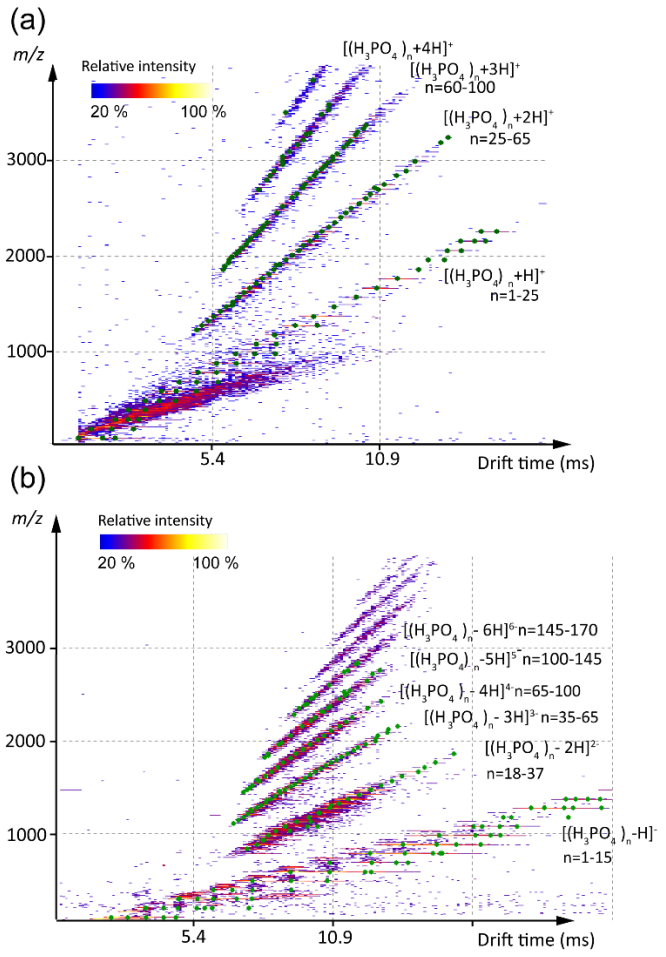

Fig. 3 (a) Positive ion mode ESI TWIM MS data obtained from a 50 mM phosphoric acid solution with 1 % mNBA. (b) Negative ion mode ESI TWIM MS data obtained from a 50 mM phosphoric acid solution with 1 % mNBA. The green dots outline the signals of phosphoric acid cluster ions (monoisotopic ions)

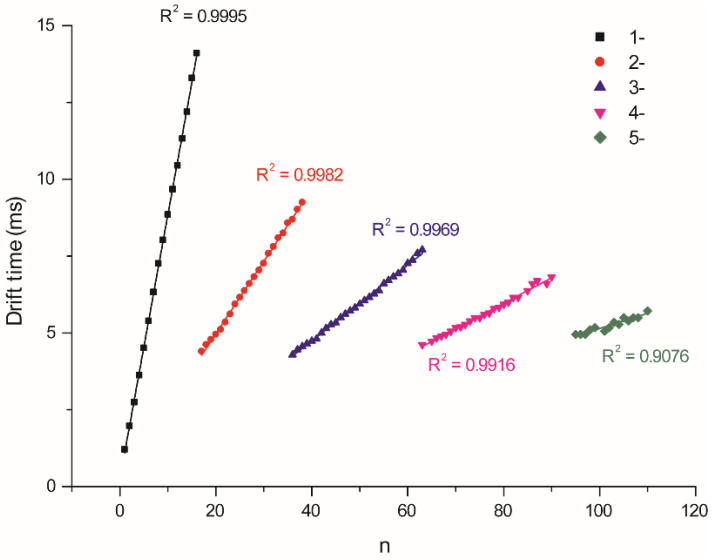

Fig. 4 Correlation of drift times with *n* for $[(H_3PO_4)_n - zH]^{z-}$ clusters for charge states (z) 1- (black squares ■), 2- (red circles ●), 3- (blue upward triangle ▲), 4- (magenta downward triangle ▼) and 5- (green diamonds ◆)

Gas phase geometries

To palliate the absence of drift tube data giving experimental collision cross sections, *ab initio* calculation using density functional theory (DFT) were carried out on $[(H_3PO_4)_n - H]^-$ cluster ions, with *n* ranging from 1 to 6. Starting from a geometry with *n* phosphoric acid molecules derived from the crystal structure, all possible *3n* deprotonation sites were tested as a means to browse the conformational space. Low energy structures are depicted in figure 5. For the negatively charged cluster ions with 1, 3, 5 and 6 phosphoric molecules, the lowest energy structure was selected. The most stable conformations were always identical from the ΔE and ΔG^0 points of view. In fact, ΔE and ΔG^0 were found to be largely correlated (R^2 = 0.99), showing temperature and entropic effects should not affect the energetic rankings.

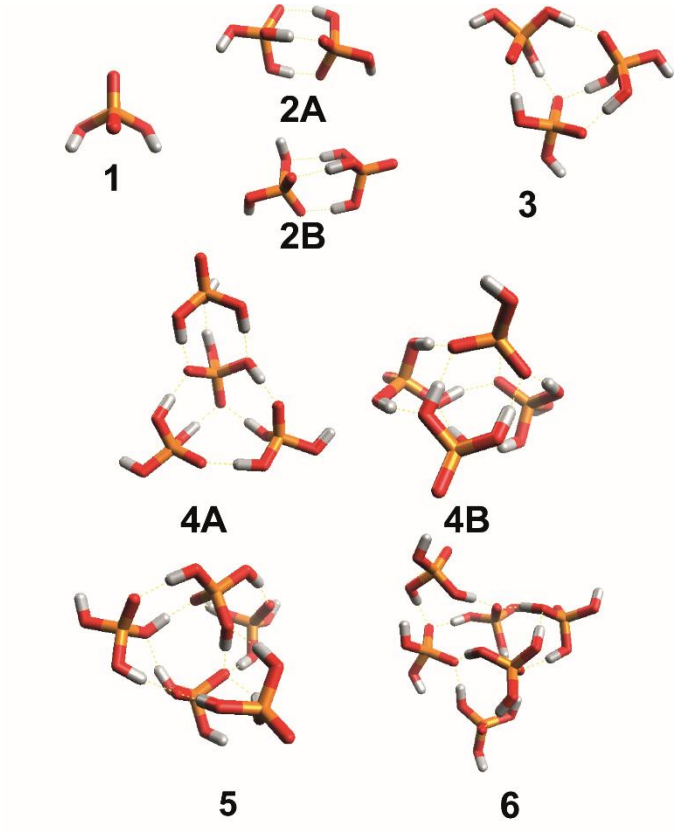

Fig. 5 Optimized lowest standard Gibbs free energy geometries (out of 3*n* starting structures) of negative cluster ions $[(H_3PO_4)_n - H]^-$, n=1 to 6

Although two to three other optimized structures came forth within a 5 kcal/mol range in terms of ΔG^0, all presented similar topological and geometrical characteristics. For the negatively charged cluster ions with 2 and 4 phosphoric acid molecules, two geometries were found within less than 2 kcal/mol (ΔG^0). For the dimer, two geometries (named 2A and 2B) within 1.5 kcal/mol from each other presented closely related geometries where only one hydrogen position differed. For the 4-mer, two geometries (4A and 4B) were within less than 1.2 kcal/mol. The lowest standard Gibbs energy structure 4A presented a rather expanded geometry with one distinctively central phosphoric acid molecule and three others around it in a roughly planar area. The other structure (4B) was an energetic minimum from the E^{ZPE} point of view and was found more globular.

We calculated interaction cross sections in helium and nitrogen gas for all *3n* optimized structures of the six negatively charged cluster ions. Different atomic charges were tested for the MOBCAL calculations: atomic polar tensor derived charges (APT) [50], charges from natural population analysis (NPA) [51] (both being obtained at a quantum level), as well as a uniform charge distribution (Equal), in order to account for possible electrostatic interactions between the analyte and the polarizable drift gas molecules. We monitored the calculated cross sections resulting of the projection approximation (PA), trajectory method (TM) and also followed the value of the structural asymmetry parameter (SAP) given by MOBCAL[40,41]. This SAP[52] is calculated by Equation 1, where d_i^{xyz} is the distance of atom *i* to the origin, and d_i^{yz} is the projected distance on plane yz while rotating the molecule by polar angles θ and φ. It is equal to 1 for spherical objects.

$$SAP = \max_{(\theta,\varphi)} \left(\frac{\pi}{4} \frac{\sum_{i=1}^{n} d_i^{xyz}}{\sum_{i=1}^{n} d_i^{yz}(\theta,\varphi)} \right)$$

Equation 1

Table 1 summarizes the values obtained for the lower energy optimized structures. Comparing the PA results for all optimized structures with the crystal starting point, we found that the gas phase structures were all more compact than the original crystal structure. For small cluster ions with one to three phosphoric acid molecules, there was around 1 to 3% relative difference for the PA cross sections. For the cluster ions with four to six phosphoric acid molecules, this relative difference increased to reach 7 to 9 % This result pointed out that the higher flexibility expected in the gas phase might, in fact, lead to more bunched arrangements than in the well-ordered solid.

Table 1. Data on the optimized lowest energy structures of of negatively charged cluster ions $[(H_3PO_4)_n - H]^-$, *n*=1 to 6 : structural asymmetry parameters (SAP) estimated dissociation energy of one phosphoric acid molecule and calculated cross sections. Comparison to the crystal-based starting structure

	Starting crystal-based structure		Optimized lowest energy structures										
								He TM			N_2 TM		
n	SAP (crystal)	PA (crystal)	Name	$\Delta(\Delta G°)$[a] kcal /mol	$\Delta(\Delta G° (-H_3PO_4))$[b] eV	SAP	PA	APT	NPA	Equal	APT	NPA	Equal
1	1.24	45.6				1.16	46.1	37.2	39.1	36.3	86.0	93.3	87.0
2	1.86	73.5	A	0.0	1.4	1.70	71.0	53.8	58.9	58.3	96.0	103.6	97.4
2			B	1.5	1.4	1.59	67.5	54.1	55.4	54.2	96.2	103.2	97.4
3	1.19	89.3			1.1	1.22	86.3	71.3	72.0	71.4	112.8	117.5	113.1
4	1.23	109.0	A	0.0	0.7	1.30	106.5	90.3	91.1	90.5	132.4	137.8	133.3
4			B	1.2	0.8	1.09	101.1	85.6	86.5	85.8	128.1	134.3	129.0
5	1.11	129.3			0.8	1.09	116.9	n.c.	n.c.	100.6	146.0	151.2	148.0
6	1.14	144.0			0.6	1.12	131.3	116.3	116.8	116.5	162.2	166.2	163.4

n.c.: no calculation. (The trajectory method could not be completed because trajectories did not verifiy energy conservation).
(a) Gibbs energy differences between structures A and B. (b) estimated dissociation energy of one phosphoric acid molecule

Monitoring the SAP of the *3n* optimized structures for each given cluster ion number, we found that different deprotonation sites led to widely different structures with SAP values that could both decrease or increase compared to the starting crystal derived geometry. For lower energy structures, however, the SAP was always lower except for the 3-mer. Among the *3n* tested conformations, it was found that the lowest energy optimized structures also presented the lowest SAP values, with the exception of the expanded 4-mer (4A) which showed a high value (1.3). With the exception of this expanded 4-mer 4A, the SAP values tended to 1.1 with increasing number of phosphoric acid molecules (Table 1). It is therefore likely that larger cluster ions could reasonably be expected spherical in shape.

Estimation of dissociation energies of the loss of one phosphoric acid molecule was carried out. The trend found showed a decrease in energy with increasing number of phosphoric acid molecules in the cluster.

Correlation of cross sections and arrival times

Choosing the structures that showed a combination of low energy and low SAP, that is excluding the expanded 4-mer 4A to privilege spherical shapes,

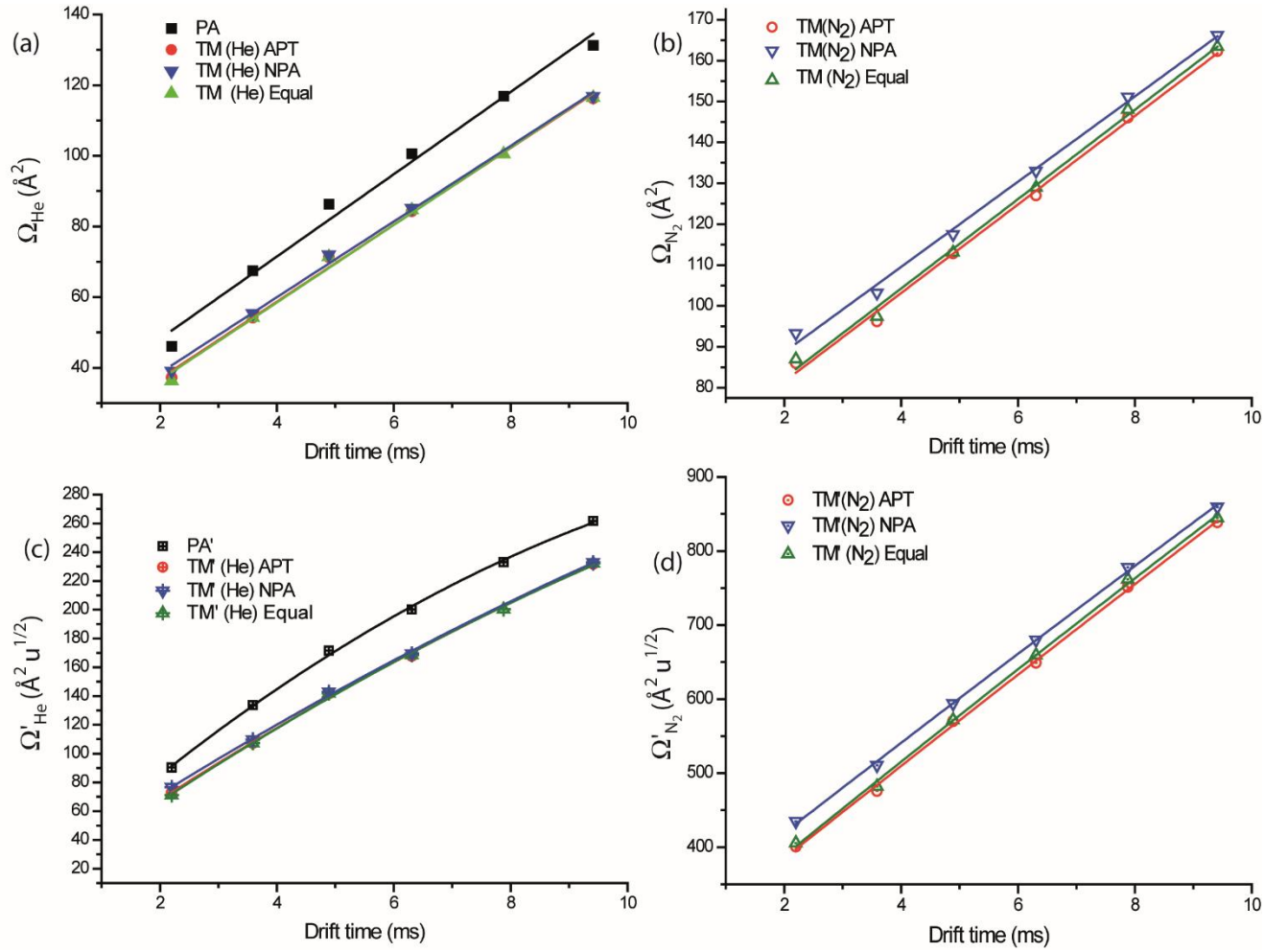

Fig. 6 Correlation tests of calculated cross sections vs experimental drift time (a) helium calculated collision cross sections, (b) nitrogen gas calculated cross sections, (c) reduced helium calculated cross sections, (d) reduced nitrogen gas calculated cross sections. Black squares are PA CCS, red circles are APT atomic charges based TM CCS, blue downward triangle are NPA atomic charges based TM CCS, green upward triangles are uniform atomic charges TM CCS

we tested a collection of statistical correlations of calculated cross sections with our experimental arrival times. Correlations with cross sections (Ω) calculated by the different methods (PA and TM), different atomic charges, with helium and nitrogen drift gases, were tested as well as correlations with the "reduced" cross sections Ω' defined by equation 2, to approach the mobility K, to which it is inversely proportional, in the low field limit.[53]

$$\Omega' = \frac{\Omega\sqrt{\mu}}{z} \quad , \quad \mu = \frac{m_{gas} m_{analyte}}{m_{gas} + m_{analyte}}$$

Equation 2

The results are shown in Figure 6. Good linear correlation was obtained in all cases as R^2 ranges from 0.985 to 0.996. With helium (Figure 6a), the TM interaction cross sections were always lower than the PA results. We found very little difference in the helium based TM interaction cross sections for the different atomic charges used in the input.

This was no longer true for interaction cross sections in nitrogen gas (Figure 6b), where relative differences between different sets of atomic charges could be as high as 7%. We also found that nitrogen gas based TM interaction cross sections with APT and NPA derived atomic charges were largely linearly correlated (R^2 = 0.998), although the atomic charges

themselves are not (R^2 = 0,01 for the atomic charge on the phosphorus atoms of the hexamer, for example). These difference were non negligible and showed it should be essential to associate one set of LJ parameters with one set of atomic charges. Indeed, although correlation did work for both sets of atomic charges, this meant that changing from one set of atomic charges to another would introduce systematic errors in the evaluation and comparison of interaction cross sections.

Although some linear correlation was observed between all calculated cross sections, we found it remarkable that the highest R^2 was obtained for TM interaction cross sections with non-uniform (either NPA or APT) atomic charges. Slightly better correlations were obtained (Table 2) when Ω_{He} was replaced by Ω_{He}', the classical transformation used by other calibration methods (Equation 1) [5,48,49].

The reduced cross sections Ω_{He}' could also be fitted to a second order polynomial equation (Figure 6c). Bush *et al.* have found multiprotonated polyalanine drift time data and the Ω_{He}/z ratio could be correlated with binomial functions [2]. Our calculated cross section data being from only singly charged ions and within a much shorter range, also showed R^2 correlation coefficient of around 0.998 with a second order polynomial fit.

When correlation was observed with nitrogen gas based calculated cross sections Ω_{N2}, the R^2 determination coefficient were close to 0.996 both with a linear function or a binomial function. Since the data was recorded with nitrogen as the buffer gas, as the TWIMS is classically operated with nitrogen gas, although some helium is present in the trap to collisionally cool the ions before the ion mobility device, we expected better correlation coefficient from the nitrogen gas based calculations [54]. The difference was very subtle, however. When Ω_{N2}' was used, the data no longer showed linear correlation, and using a second order polynomial equation did not allow to reach similar R^2 values.

Table 2. Correlation coefficient R^2 for different curve fitting schemes of calculated cross section versus experimental drift times.

		PA	TM		
			APT	NPA	Equal
Ω_{He}	Linear fit	0.9861	0.9949	0.9962	0.9946
	Binomial fit	0.9979	0.9981	0.9984	0.9985
Ω'_{He}	Linear fit	0.9856	0.9980	0.9985	0.9978
	Binomial fit	0.9984	0.9980	0.9985	0.9981
Ω_{N2}	Linear fit		0.9958	0.9955	0.9959
	Binomial fit		0.9963	0.9967	0.9960
Ω'_{N2}	Linear fit		0.9988	0.9992	0.9988
	Binomial fit		0.9984	0.9990	0.9985

Conclusion

Phosphoric acid clusters showed a good potential for use in ion mobility mass spectrometry experiments. Phosphoric acid, a very inexpensive and accessible compound, formed hydrogen bonded cluster both in the positive and negative ion mode, which were easily obtained and separated according to charge state in the *m/z* versus arrival time maps. The charge states ranged from 1 to 4 in the positive ion mode and 1 to 6 in the negative ion mode and covered the *m/z* range from roughly 100 to 3000 with a 50 mM phosphoric acid solution. Such range could probably be expanded with higher concentrations and supercharging agents.

Phosphoric acid solutions can be used to tune the experimental parameters in ion mobility mass spectrometry experiments by monitoring the dissociation of cluster ions. Instrumental settings that minimize the cleavage of hydrogen bonds should also increase the probability of non-covalent interactions retention in native peptides and proteins.

With carefully tuned experimental parameters, phosphoric acid cluster ions lead to regularly spaced data in the m/z versus drift time map showing a good potential for the calibration of traveling wave ion mobility devices for measurements of cross sections. For now, no drift tube ion mobility derived cross

sections exist for phosphoric acid cluster ions, however.

By performing *ab initio* calculations, although limited here to the smallest negatively charged multimers, we confirmed that the clusters are expected to be nearly spherical, especially for larger clusters. The estimation of cross sections from our calculated structures showed the need for reference data to parameterize the LJ potentials of the trajectory method as a function of the type of atomic charges used in the input, especially for nitrogen gas based calculations.

No doubt, this deficit of experimental and reference data should disappear in time, as the need for standards for the proteomic and metabolomics databases is strong. Although, trends tend toward the use of similar molecules to measure cross section within one family of compounds, the use of one well characterized and versatile calibrant might help also bring better consensus to ion mobility measurements.

Acknowledgements

The authors gratefully acknowledge the Région Haute-Normandie, the Labex SynOrg (ANR-11-LABX-0029) and the European Regional Development Fund (ERDF 31708) for financial support and the Centre de Ressources Informatiques de Haute-Normandie (CRIHAN) for computational time. VT thanks the Centre National de la Recherche Scientifique (CNRS) for a “chaire d’excellence” at the University of Rouen. Thanks also to Samuel Petit for his help on the crystallographic data.

References

1. Shvartsburg, A.A., Smith, R.D.: Fundamentals of Traveling Wave Ion Mobility Spectrometry. *Anal. Chem.* **80**, 9689-9699 (2008).
2. Bush, M.F., Campuzano, I.D.G., Robinson, C.V.: Ion Mobility Mass Spectrometry of Peptide Ions: Effects of Drift Gas and Calibration Strategies. *Anal. Chem.* **84**, 7124-7130 (2012).
3. Smith, D.P., Knapman, T.W., Campuzano, I., Malham, R.W., Berryman, J.T., Radford, S.E., Ashcroft, A.E.: Deciphering drift time measurements from travelling wave ion mobility spectrometry-mass spectrometry studies. *Eur. J. Mass Spectrom.* **15**, 113-130 (2009).
4. Bush, M.F., Hall, Z., Giles, K., Hoyes, J., Robinson, C.V., Ruotolo, B.T.: Collision Cross Sections of Proteins and Their Complexes: A Calibration Framework and Database for Gas-Phase Structural Biology. *Anal. Chem.* **82**, 9557-9565 (2010).
5. Ruotolo, B.T., Benesch, J.L.P., Sandercock, A.M., Hyung, S.-J., Robinson, C.V.: Ion mobility-mass spectrometry analysis of large protein complexes. *Nat. Protoc.* **3**, 1139-1152 (2008).
6. Salbo, R., Bush, M.F., Naver, H., Campuzano, I., Robinson, C.V., Pettersson, I., Jorgensen, T.J.D., Haselmann, K.F.: Traveling-wave ion mobility mass spectrometry of protein complexes: accurate calibrated collision cross-sections of human insulin oligomers. *Rapid Commun. Mass Spectrom.* **26**, 1181-1193 (2012).
7. Silveira, J.A., Jeon, J., Gamage, C.M., Pai, P.-J., Fort, K.L., Russell, D.H.: Damping Factor Links Periodic Focusing and Uniform Field Ion Mobility for Accurate Determination of Collision Cross Sections. *Anal. Chem.* **84**, 2818-2824 (2012).
8. Dwivedi, P., Schultz, A.J., Hill, H.H.: Metabolic Profiling of Human Blood by High Resolution Ion Mobility Mass Spectrometry (IM-MS). *Int. J. Mass Spectrom.* **298**, 78-90 (2010).
9. Ahmed, A., Cho, Y.J., No, M.-h., Koh, J., Tomczyk, N., Giles, K., Yoo, J.S., Kim, S.: Application of the Mason-Schamp Equation and Ion Mobility Mass Spectrometry To Identify Structurally Related Compounds in Crude Oil. *Anal. Chem.* **83**, 77-83 (2011).
10. McLean, J.A., Ruotolo, B.T., Gillig, K.J., Russell, D.H.: Ion mobility-mass spectrometry: a new paradigm for proteomics. *Int. J. Mass Spectrom.* **240**, 301-315 (2005).
11. Tao, L., McLean, J.R., McLean, J.A., Russell, D.H.: A collision cross-section database of singly-charged peptide ions. *J. Am. Soc. Mass Spectrom.* **18**, 1232-1238 (2007).
12. Leary, J.A., Schenauer, M.R., Stefanescu, R., Andaya, A., Ruotolo, B.T., Robinson, C.V., Thalassinos, K., Scrivens, J.H., Sokabe, M., Hershey, J.W.B.: Methodology for Measuring Conformation of Solvent-Disrupted Protein Subunits using T-WAVE Ion Mobility MS: An Investigation

into Eukaryotic Initiation Factors. *J. Am. Soc. Mass Spectrom.* **20**, 1699-1706 (2009).
13. Michaelevski, I., Eisenstein, M., Sharon, M.: Gas-Phase Compaction and Unfolding of Protein Structures. *Anal. Chem. (Washington, DC, U. S.)* **82**, 9484-9491 (2010).
14. Zhang, D., Cooks, R.G.: Doubly charged cluster ions [(NaCl)m(Na)2]2+: magic numbers, dissociation, and structure. *Int. J. Mass Spectrom.* **195–196**, 667-684 (2000).
15. Schroder, D.: Ion clustering in electrospray mass spectrometry of brine and other electrolyte solutions. *Phys. Chem. Chem. Phys.* **14**, 6382-6390 (2012).
16. Zhou, S., Hamburger, M.: Formation of Sodium Cluster Ions in Electrospray Mass Spectrometry. *Rapid Commun. Mass Spectrom.* **10**, 797-800 (1996).
17. Nanita, S.C., Cooks, R.G.: Serine octamers: cluster formation, reactions, and implications for biomolecule homochirality. *Angew. Chem., Int. Ed.* **45**, 554-569 (2006).
18. Galhena, A.S., Jones, C.M., Wysocki, V.H.: Influence of cluster size and ion activation method on the dissociation of cesium iodide clusters. *Int. J. Mass Spectrom.* **287**, 105-113 (2009).
19. Hao, C., March, R.E.: Electrospray ionization tandem mass spectrometric study of salt cluster ions: part 2--salts of polyatomic acid groups and of multivalent metals. *J. Mass Spectrom.* **36**, 509-521 (2001).
20. Zatula, A.S., Ryding, M.J., Andersson, P.U., Uggerud, E.: Proton mobility and stability of water clusters containing alkali metal ions. *Int. J. Mass Spectrom.* **330-332**, 191-199 (2012).
21. Sobott, F., Hernández, H., McCammon, M.G., Tito, M.A., Robinson, C.V.: A Tandem Mass Spectrometer for Improved Transmission and Analysis of Large Macromolecular Assemblies. *Anal. Chem.* **74**, 1402-1407 (2002).
22. Myung, S., Fioroni, M., Julian, R.R., Koeniger, S.L., Baik, M.H., Clemmer, D.E.: Chirally directed formation of nanometer-scale proline clusters. *J. Am. Chem. Soc.* **128**, 10833-10839 (2006).
23. Jarrold, M.F.: Drift Tube Studies of Atomic Clusters. *J. Phys. Chem.* **99**, 11-21 (1995).
24. Weis, P.: Structure determination of gaseous metal and semi-metal cluster ions by ion mobility spectrometry. *Int. J. Mass Spectrom.* **245**, 1-13 (2005).
25. Weis, P., Gilb, S., Gerhardt, P., Kappes, M.M.: A time-of-flight, drift cell, quadrupole apparatus for ion mobility measurements. *Int. J. Mass Spectrom.* **216**, 59-73 (2002).
26. Ouyang, H., Larriba-Andaluz, C., Oberreit, D.R., Hogan, C.J., Jr.: The Collision Cross Sections of Iodide Salt Cluster Ions in Air via Differential Mobility Analysis-Mass Spectrometry. *J. Am. Soc. Mass Spectrom.*, 10.1007/s13361-013-0724-8 (2013).
27. Rajbanshi, A., Wan, S., Custelcean, R.: Dihydrogen Phosphate Clusters: Trapping H2PO4–Tetramers and Hexamers in Urea-Functionalized Molecular Crystals. *Cryst. Growth Des.* **13**, 2233-2237 (2013).
28. Hossain, M.A., Isiklan, M., Pramanik, A., Saeed, M.A., Fronczek, F.R.: Anion Cluster: Assembly of Dihydrogen Phosphates for the Formation of a Cyclic Anion Octamer. *Cryst. Growth Des.* **12**, 567-571 (2012).
29. Vilciauskas, L., Paddison, S.J., Kreuer, K.D.: Ab initio modeling of proton transfer in phosphoric acid clusters. *J. Phys. Chem. A* **113**, 9193-9201 (2009).
30. Kong, X.: Serine-phosphoric acid cluster ions studied by electrospray ionization and tandem mass spectrometry. *J. Mass Spectrom.* **46**, 535-545 (2011).
31. Sammes, N., Bove, R., Stahl, K.: Phosphoric acid fuel cells: Fundamentals and applications. *Current Opinion in Solid State and Materials Science* **8**, 372-378 (2004).
32. Knapman, T.W., Berryman, J.T., Campuzano, I., Harris, S.A., Ashcroft, A.E.: Considerations in experimental and theoretical collision cross-section measurements of small molecules using travelling wave ion mobility spectrometry-mass spectrometry. *Int. J. Mass Spectrom.* **298**, 17-23 (2010).
33. Lapthorn, C., Pullen, F., Chowdhry, B.Z.: Ion mobility spectrometry-mass spectrometry (IMS-MS) of small molecules: separating and assigning structures to ions. *Mass Spectrom. Rev.* **32**, 43-71 (2013).
34. Lapthorn, C., Dines, T.J., Chowdhry, B.Z., Perkins, G.L., Pullen, F.S.: Can ion mobility mass spectrometry and density functional theory help elucidate protonation sites in 'small' molecules? *Rapid Commun. Mass Spectrom.* **27**, 2399-2410 (2013).
35. Frisch, M.J., Trucks, G.W., Schlegel, H.B., Scuseria, G.E., Robb, M.A., Cheeseman, J.R., Scalmani, G., Barone, V., Mennucci, B., Petersson, G.A., Nakatsuji, H., Caricato, M., Li, X., Hratchian, H.P., Izmaylov, A.F., Bloino, J., Zheng, G., Sonnenberg, J.L., Hada, M., Ehara, M., Toyota, K., Fukuda, R., Hasegawa, J., Ishida, M., Nakajima, T., Honda, Y., Kitao, O., Nakai, H., Vreven, T., Montgomery. Jr, J.A., Peralta, J.E., Ogliaro, F., Bearpark, M., Heyd, J.J., Brothers, E., Kudin, K.N., Staroverov, V.N., Kobayashi, R., Normand, J., Raghavachari, K., Rendell, A., Burant, J.C., Iyengar, S.S., Tomasi, J., Cossi, M., Rega, N., Millam, N.J., Klene, M., Knox, J.E., Cross, J.B., Bakken, V., Adamo, C., Jaramillo, J.,

Gomperts, R., Stratmann, R.E., Yazyev, O., Austin, A.J., Cammi, R., Pomelli, C., Ochterski, J.W., Martin, R.L., Morokuma, K., Zakrzewski, V.G., Voth, G.A., Salvador, P., Dannenberg, J.J., Dapprich, S., Daniels, A.D., Farkas, Ö., Foresman, J.B., Ortiz, J.V., Cioslowski, J., Fox, D.J.; Gaussian09, Revision D.01 ; Gaussian, Inc.: Wallingford CT, 2009.

36. Chai, J.D., Head-Gordon, M.: Long-range corrected hybrid density functionals with damped atom-atom dispersion corrections. *Phys. Chem. Chem. Phys.* **10**, 6615-6620 (2008).

37. Souhassou, M., Espinosa, E., Lecomte, C., Blessing, R.H.: Experimental electron density in crystalline H3PO4. *Acta Crystallographica Section B Structural Science* **51**, 661-668 (1995).

38. Bergerhoff, G.B., I.D. In *International Union of Crystallography*; (Hrsg.), F. H. A. e. a., Ed. Chester, 1987.

39. Belsky, A., Hellenbrandt, M., Karen, V.L., Luksch, P.: New developments in the Inorganic Crystal Structure Database (ICSD): accessibility in support of materials research and design. *Acta Crystallographica Section B Structural Science* **58**, 364-369 (2002).

40. Mesleh, M.F., Hunter, J.M., Shvartsburg, A.A., Schatz, G.C., Jarrold, M.F.: Structural Information from Ion Mobility Measurements: Effects of the Long-Range Potential. *J. Phys. Chem.* **100**, 16082-16086 (1996).

41. Shvartsburg, A.A., Jarrold, M.F.: An exact hard-spheres scattering model for the mobilities of polyatomic ions. *Chem. Phys. Lett.* **261**, 86-91 (1996).

42. Campuzano, I., Bush, M.F., Robinson, C.V., Beaumont, C., Richardson, K., Kim, H., Kim, H.I.: Structural Characterization of Drug-like Compounds by Ion Mobility Mass Spectrometry: Comparison of Theoretical and Experimentally Derived Nitrogen Collision Cross Sections. *Anal. Chem.* **84**, 1026-1033 (2012).

43. Giles, K., Wildgoose, J.L., Langridge, D.J., Campuzano, I.: A method for direct measurement of ion mobilities using a travelling wave ion guide. *Int. J. Mass Spectrom.* **298**, 10-16 (2010).

44. Morsa, D., Gabelica, V., De Pauw, E.: Effective Temperature of Ions in Traveling Wave Ion Mobility Spectrometry. *Anal. Chem.* **83**, 5775-5782 (2011).

45. Iavarone, A.T., Williams, E.R.: Supercharging in electrospray ionization: effects on signal and charge. *Int. J. Mass Spectrom.* **219**, 63-72 (2002).

46. Damen, C.W.N., Chen, W., Chakraborty, A.B., van Oosterhout, M., Mazzeo, J.R., Gebler, J.C., Schellens, J.H.M., Rosing, H., Beijnen, J.H.: Electrospray Ionization Quadrupole Ion-Mobility Time-of-Flight Mass Spectrometry as a Tool to Distinguish the Lot-to-Lot Heterogeneity in N-Glycosylation Profile of the Therapeutic Monoclonal Antibody Trastuzumab. *J. Am. Soc. Mass Spectrom.* **20**, 2021-2033 (2009).

47. Maire, F., Neeson, K., Denny, R., McCullagh, M., Lange, C., Afonso, C., Giusti, P.: Identification of ion series using ion mobility mass spectrometry: the example of alkyl-benzothiophene and alkyl-dibenzothiophene ions in Diesel fuels. *Anal. Chem.* **85**, 5530-5534 (2013).

48. Smith, D.P., Knapman, T.W., Campuzano, I., Malham, R.W., Berryman, J.T., Radford, S.E., Ashcroft, A.E.: Deciphering drift time measurements from travelling wave ion mobility spectrometry-mass spectrometry studies. *Eur J Mass Spectrom (Chichester, Eng)* **15**, 113-130 (2009).

49. Thalassinos, K., Grabenauer, M., Slade, S.E., Hilton, G.R., Bowers, M.T., Scrivens, J.H.: Characterization of phosphorylated peptides using traveling wave-based and drift cell ion mobility mass spectrometry. *Anal. Chem.* **81**, 248-254 (2009).

50. Cioslowski, J.: A new population analysis based on atomic polar tensors. *J. Am. Chem. Soc.* **111**, 8333-8336 (1989).

51. Reed, A.E., Curtiss, L.A., Weinhold, F.: Intermolecular interactions from a natural bond orbital, donor-acceptor viewpoint. *Chem. Rev. (Washington, DC, U. S.)* **88**, 899-926 (1988).

52. Kinnear, B.S., Kaleta, D.T., Kohtani, M., Hudgins, R.R., Jarrold, M.F.: Conformations of Unsolvated Valine-Based Peptides. *J. Am. Chem. Soc.* **122**, 9243-9256 (2000).

53. Mason, E.A., McDaniel, E.W. *Transport Properties of Ions in Gases*; Wiley: New York, 1988.

54. Giles, K., Williams, J.P., Campuzano, I.: Enhancements in travelling wave ion mobility resolution. *Rapid Commun. Mass Spectrom.* **25**, 1559-1566 (2011).